A Metal-Organic Framework Based on a Tetra-Arylextended Calix[4]pyrrole Ligand: Structure Control through the Covalent Connectivity in the Linker.

Jordi Aguilera-Sigalat,[a] Cristina Sáenz de Pipaón,[a] Daniel Hernández-Alonso,[a] Eduardo C. Escudero-Adán,[a] José Ramón Galan-Mascarós,[a,b] Pablo Ballester*[a,b]*

[a] Institute of Chemical Research of Catalonia (ICIQ), The Barcelona Institute of Science and Technology, Avgda. Països Catalans 16, 43007 Tarragona, Spain.

[b] ICREA, Passeig Lluís Companys, 23, 03018 Barcelona, Spain

ABSTRACT. The preparation of isomeric metal-organic frameworks in which the network topology is controlled by the different covalent connectivity of the organic ligand is an important step forward in the design of new functional materials. In this context, macrocyclic organic ligands able to accommodate suitable guests in their own polar internal cavities are appealing candidates to act as multidentate linkers, which could potentially self-assemble into hierarchical porous

structures. Taking this into account, here we report the first successful attempt to incorporate a tetraaryl-extended calix[4]pyrrole derivative into a transition metal-organic framework (**MOF1**) by simply incorporating four terminal carboxylic functional groups at the upper rim of the macrocyclic scaffold. Remarkably, the structures of the metal organic framework and its transition-metal carboxylate clusters (secondary building units, SBU) are governed by the position of the carboxylic substituent in the functionalized *meso*-aryl units of the linker. Only the tetra-α–*meso*-arylextended tetracarboxylic calix[4]pyrrole isomer **L1**, substituted in a single *meta*-position of their aryl rings, yields a 2-D MOF architecture assembled through complex Cu^{II}-carboxylate clusters (SBU). The clusters have higher nuclearity than the Cu^{II}_2-$(O_2CR)_4$ paddle wheels produced as SBUs during the assembly of the *para*-substituted counterpart **L2**. Remarkably, the length of the dialkylformamide used as solvent (DMF or DEF) in the synthesis of the Cu^{II}-organic materials derived from **L2** played a key role in the structure of the final solid material. The packing of discrete metal-mediated capsular dimers of **L2** switched to that of 1-D linear coordination polymers when the solvent's alkyl chains were increased by a methylene unit. Finally, ligand **L3**, which featured a longer alkyl spacer between the *para*-substituted calix[4]pyrrole core and the terminal carboxylic groups than **L2**, self-assembled, exclusively, into discrete capsular coordination dimers also mediated by Cu^{II} paddle wheel units.

1. INTRODUCTION

Metal-organic frameworks (MOFs), also referred to as porous coordination polymers, are a class of hybrid materials built from metals ions (or clusters) and polydentate organic ligands (linkers).[1,2] These crystalline materials with high surface areas and ideally permanent porosity have been used in a wide range of applications, such as gas storage and separation,[3] sensing[4] or catalysis,[5] among

others. The vast choice of organic ligands allows infinite possibilities for the preparation of MOFs where the structure-properties relationship can be modulated accordingly.

The design of the structure's ligand plays a key role in the preparation of these materials, which could endow their porosity with a hierarchical configuration, which is with different pore sizes: large resulting from the MOF framework and small defined by the ligand's structure. In addition, the ligand's structure could also confer a certain degree of conformational flexibility to the MOF that might be promoted via an external stimuli, such as the response to guests' addition or light.[6,7,8] The effect exerted by the position and length of the ligand's substituent on the structure of the resulting metal-organic framework has been demonstrated.[9] For instance, Chen *et al.*[10] reported the influence of the substituent's length when using an imidazole ligand. Thus, when 2-methylimidazole was employed, a sodalite-type MOF structure was obtained, whereas changing to 2-ethylimidazole led to a zeolitic analcime MOF topology; in other cases, when unsubstituted imidazole was used, a chain-like structure was assembled.[11] Very recently, Dalgarno *et al.*[12] reported the effect of the substituent position on the assembly of metal-organic structures based on xylyl bis-calix[4]arene ligands. They observed that while *ortho*- and *meta*-xylyl bis-calix[4]arenes formed clusters with Fe^{III} and Ln^{III} metal centers, the *para*-xylyl bis-calix[4]arene derivative yielded a trigonal antiprismatic metal-organic cage that showed good thermal stability and partial N_2 and H_2 uptake.

The effect of the solvent in the design and/or functionalization of MOFs is also well known. In this context, postsynthetic ligand exchange methodologies (PSLE), also referred as solvent-assisted ligand exchange (SALE), have shown high solvent-dependence during the linker exchange process of the pre-synthetized metal-organic framework. Several authors have dwelt on this subject.[13,14] On the other hand, the effect produced by the solvent during the crystallization

processes involved in the MOFs syntheses is also important. It was shown that solvent polarity effects modulate the conformation of the resulting polymeric structure, as reported by Chen *et al.* [15] in the production of "supramolecular isomers".[16] The differences in solvent polarity modulate the supramolecular interactions that exist between the organic linkers and the solvent molecules, which in turn endows the metal frameworks with different local coordination geometries.

Calix[4]pyrroles are a class of macrocyclic compounds formed by four pyrrole units linked through a doubly substituted sp^3 hybridized carbon, the so-called *meso*-carbon.[17,18] The structural versatility and functionality displayed by these compounds makes them attractive candidates to function as molecular receptors. These molecules show high affinity towards anions and neutral molecules having electron-rich groups. Calix[4]arenes are structurally related to calix[4]pyrroles. The former have also played a key role in the development of molecular recognition strategies. Several studies described the construction of MOFs containing calix[4]arenes as linker units.[19] The first study, reported by Zhang *et al.*,[20] described two 3-D framework constructed from tetra-*p*-sulfonatocalix[4]arenes and rare earth cations (*i.e.* Nd^{III} and Eu^{III}). Subsequently, Dalgarno *et al.*[21] described the preparation of *p*-carboxylatocalix[4]arene-based MOFs in which the switching of the assembly process from 1D to 3D scaffolds was governed by steric effects of the ligands. Thurston *et al*.[22] proposed the synthesis of calix[4]arene containing MOFs in order to build hierarchical porous structures. However, only theoretical simulations were performed due to lack of success in the activation of the synthesized assemblies. In this context, Park *et al.*[23] reported the synthesis and subsequent activation of a $[(Pb_2@L) \times 2\ DMF]_n$ MOF, where L is a carboxylic acid-functionalized calix[4]arene, which involves a single-crystal to single-crystal transformation upon solvent removal.

Regarding calix[4]pyrrole ligands, to the best of our knowledge there is only one very recent report dealing with the preparation of a MOF by combining praseodymium clusters with conformationally flexible two-wall aryl-extended calix[4]pyrroles. The two-component assembly resulted in a 3-D structure containing free struts in the 1D channels of the framework. The authors took advantage of the high affinity of the fluoride anion for the pyrrole NHs of the calixpyrrole. The binding of the anion induced a change in the conformation of the calix[4]pyrrole scaffold: from 1,3 alternate to cone-conformation. This conformational change provoked the disassembly of the MOF network and the consequent release of the entrapped molecules.[24] The possibility that the breakup of the praseodymium MOF might also be mediated or assisted by the formation of praseodymium fluoride complexes cannot be ruled out.

Hence, owing to the experience of our group on the preparation of functionalized two- and four-wall aryl-extended calix[4]pyrroles and the potential applications of calix[4]pyrrole-based MOFs for selective molecular recognition and sensing, we focused our efforts on the synthesis and study of unprecedented MOFs based on four wall aryl-extended calix[4]pyrrole scaffolds. The capability of metal ions or ion-cluster to direct multiple structures of coordination frameworks is well established. We selected Cu^{II} salts as precursors of the secondary binding units (SBUs) in the metal-organic structures, owing to their well-known properties to form different Cu^{II}-clusters by coordination with carboxylate groups. Here, we report four novel metal-organic materials, **MOF1**, **CP2**, and the discrete capsular dimers **C2** and **C3**. On the one hand, the tetracarboxylic *meta*-substituted four wall aryl-extended calix[4]pyrrole **L1** produced **MOF1**. On the other hand, the *para*-substituted isomer, **L2**, afforded either a coordination polymer, **CP2**, or a discrete capsular dimer **C2** depending on the solvent used in the solvothermal synthesis, DMF or DEF respectively. The use of the **L3** ligand, also featuring *para*-substitution in the aryl-extended calix[4]pyrrole core

but with a longer alkyl spacer spanning the distance between the terminal carboxylic groups and the *meso*-phenoxy substituents, exclusively produced a discrete capsular dimer **C3**. The Cu^{II}-carboxylate clusters acting as secondary binding units (SBUs) in **CP2**, **C2** and **C3** had Cu^{II}_2-$(O_2CR)_4$ paddle wheel structure. Conversely, the **MOF1** featured a more complex metal cluster as SBU, which comprised four Cu^{II} centers bridged by two μ_3-OH ligands giving rise to two-edge sharing $Cu^{II}_3(OH)$ triangles. The Cu^{II} ions were 3- and 4- coordinate. Our results demonstrate the viability of building metal-organic structures based on tetraaryl-extended calix[4]pyrroles. Additionally, we obtained a variety of topologies in their crystal structures, which are controlled by the position of the substituent in the *meso*-aryl rings of the organic linkers, the substituent's length, and, in one example, the size of the dialkylformamide used as solvent in the synthesis. Our findings also showcase the versatility and flexibility featured by calix[4]pyrrole-based metal-organic networks. Indeed, the reported materials demonstrate, for the first time, how significant changes in topology and morphology of metal-networks can be achieved by employing different isomeric calix[4]pyrrole ligands as building block.

Scheme 1. Preparation of the different calix[4]pyrrole-based metal-organic assemblies.

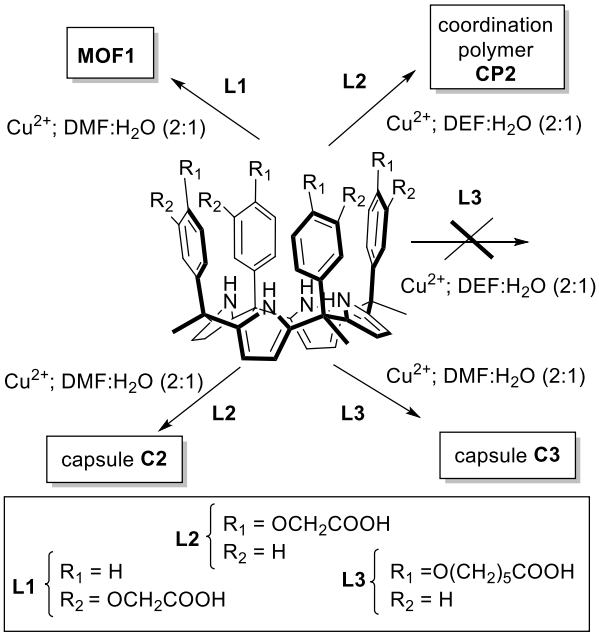

2. RESULTS

2.1. Synthesis. We explored the formation of metal-organic compounds using three different *meso*-tetraaryl *meso*-tetramethyl calix[4]pyrrole tetracarboxylic acid derivatives: **L1**: a tetra-α-calix[4]pyrrole isomer bearing a *meta*-substituted aryl group geminal to the methyl group in each one of the four *meso*-carbons. The *meta*-substituent is a 2-oxy-acetic acid; **L2**, a regio-isomer of **L1** with the 2-oxy-acetic acid substituent attached to the *para*- position of the *meso*-aryl groups; and **L3**, containing the basic tetra-*α meso*-tetraaryl *meso*-tetramethyl calix[4]pyrrole structure but featuring a 6-oxy-*n*-hexanoicacid as substituent in the *para*-position of the *meso*-aryl units.

Solvothermal reaction of the three different calix[4]pyrrole derivatives, **L1**, **L2** and **L3**, was attempted with metal salts of Cu^{II}. Successful reactions yielding unique crystalline products (Scheme 1) were found to follow an analogous procedure: heating the mixture of the ligand and the Cu^{II} salt in a Teflon-lined autoclave at 100 ºC for 24 h and subsequent cooling at room temperature provided a blue crystalline powder that was isolated by filtration, washed with dimethyl formamide (DMF) and ethanol and dried at 80 ºC for 24 h. We found that the crystallinity

of the material increased if a layer of water was placed on the bottom of the reactor and was carefully covered with the DMF solution containing both the salt and the calix[4]pyrrole ligand prior to solvothermal treatment. Using this methodology, single crystals suitable for X-Ray diffraction analysis were obtained, most likely due to the slow diffusion of the DMF into the water phase. Control experiments carried out in the absence of water or in a homogeneous DMF/H_2O mixture did not afford crystalline materials. The single crystals obtained in layered reaction conditions correspond to an extended coordination network (**MOF1)** for **L1**, and the cage-like coordination compounds using **L2** and **L3** (**C2** and **C3**, respectively, *vide infra*). By replacing DMF by diethylformamide (DEF), a polymeric structure **CP2** was also obtained starting from **L2**. Taken together, these results demonstrate the importance of the solvent in the synthesis of these metal-organic materials. Remarkably, for the **L3** ligand the change of solvent did not favor the formation of any crystalline metal-organic material.

2.2. Crystal structures.

2.2.1 MOF1 and CP2. The crystal structure of the **MOF1** is formed by extended coordination layers on the *ab* axis, yielding a 2D-like material.[25] The layers are built from [Cu_4OH_2] moieties, where the Cu^{II} atoms form a rhomb, with the two hydroxy groups located at the center of each triangle (Figure 1a) defined by the sides and the short diagonal. These hydroxy units are not coplanar, and appear one above and one below the plane defined by the four Cu^{II} atoms. The two Cu^{II} atoms at the short diagonal (Cu–Cu distance = 2.868 Å) are connected through this double hydroxy bridge, and complete their pseudo-square planar coordination geometry with two carboxylate groups, from two different calix units. These carboxylate groups show a *syn-syn* geometry and bridge the Cu^{II} atoms in the short diagonal to the Cu^{II} atoms in the long diagonal, displaying a syn-syn coordination mode (Cu–Cu distance = 3.296 Å). The Cu^{II} atoms in the long

diagonal complete their distorted trigonal bipyramid geometry with one oxygen atom of a terminal carboxylate group from an additional calix ligand and another oxygen atom of one carboxylic group of a fourth calix linker. In this way, each [Cu_4OH_2] is connected to eight different calix units, four above and four below the plane defined by the short diagonal copper centers (Figure 1b). Each calix unit binds four tetracopper clusters, forming a pseudotetragonal packing in the layers (Figure 1c). The center of symmetry at the center of the [Cu_4] rhomb imposes an eclipsed conformation for the ligands at both sides of the mean plane, and between all layers (Figure 1d). The 2D layers are packed though DMF molecules, with one methyl group facing the lower rim of the calix[4]pyrroles. The four pyrrole NH groups point towards the calix cavity, strongly binding a solvent DMF molecule and establishing four simultaneous hydrogen bonds with the oxygen atom. Disordered solvent molecules occupy the empty voids in the crystal.

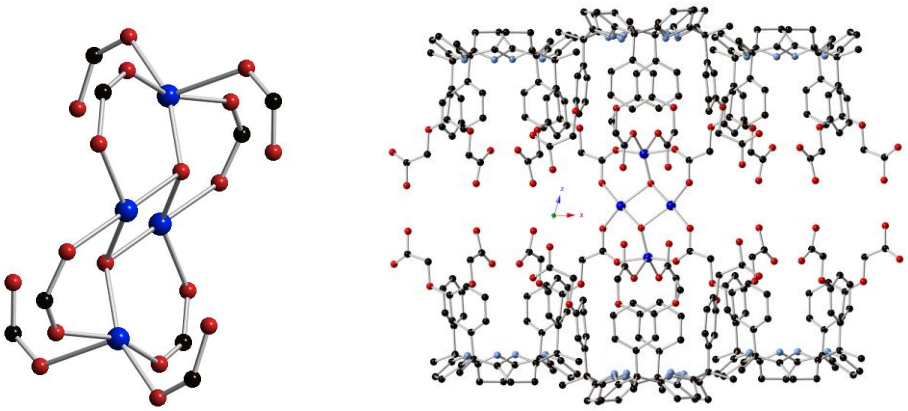

a) b)

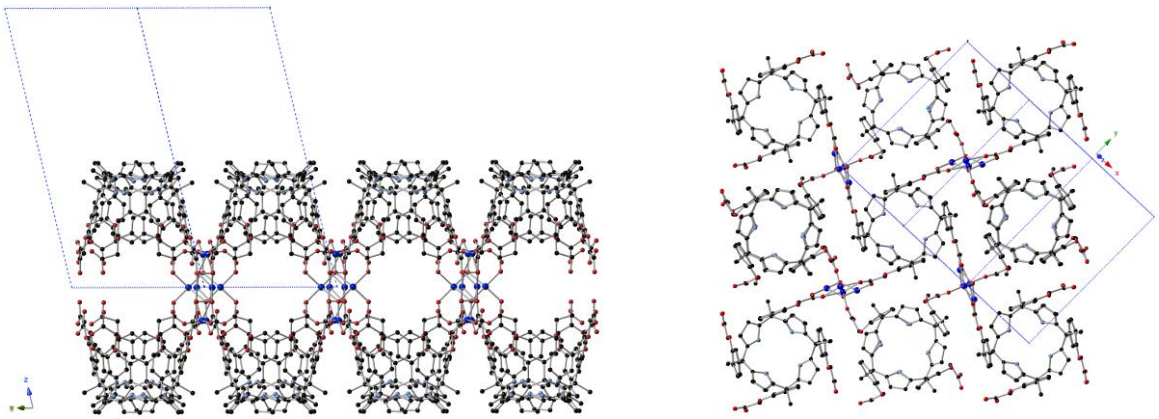

c) d)

Figure 1. Representation of the crystal structure of **MOF1**: a) Detail of the Cu_4 tetramer with its coordination geometry. b) Projection on the *ac* plane of a Cu^{II}_4 tetramer with all the coordinating ligands. c) Projection on the *ac* plane of the layered structure. d) Projection on the *ab* plane.

T**able 1.** Crystallographic data and main refinement parameters.

	MOF1	**CP2**	**C2**	**C3**
Formula	$C_{128.5}H_{138}Cu_4N_{13.5}O_{33.5}$	$C_{66}H_{76}Cu_2N_6O_{17}$	$C_{62}H_{62}Cu_2N_6O_{15.5}$	$C_{159}H_{195}Cu_4N_{13}O_{29}$
M_w	2661.68	1352.40	1266.25	3006.43
T (K)	90(2)	100(2)	100(2)	100(2)
Crystal system	Triclinic	Orthorhombic	Orthorhombic	Triclinic
Space group	$P\bar{1}$	P*bcm*	P*mna*	$P\bar{1}$
a (Å)	16.241(2)	12.3540(6)	21.9220(6)	17.8930(4)
b (Å)	16.868(3)	23.2173(12)	23.5108(8)	20.4413(5)
c (Å)	26.290(2)	21.5694(8)	23.6094(7)	21.0342(5)
α (º)	89.457(10)	90	90	79.281(2)
β (º)	72.01(2)	90	90	84.283(2)
γ (º)	88.243(14)	90	90	75.326(2)

V (Å^3)	6847.0(17)	6186.7(5)	12168.4(6)	7301.4(3)
Z	2	4	8	2
ρ_{calc} (g/cm^3)	1.291	1.452	1.382	1.367
μ (mm^{-1})	0.690	0.765	0.771	0.654
F (000)	2775	2832	5264	3176
2θ range (º)	4.056 to 42.236	4.184 to 51.364	4.284 to 50.698	3.652 to 61.290
Index range	$-16 \le h \le 16$	$-14 \le h \le 14$	$-25 \le h \le 26$	$-25 \le h \le 25$
	$-17 \le k \le 17$	$-25 \le k \le 28$	$-28 \le k \le 28$	$-29 \le k \le 29$
	$-26 \le l \le 26$	$-26 \le l \le 26$	$-27 \le l \le 28$	$-27 \le l \le 27$
Reflections$_{total}$	26238	33340	105910	171725
Reflections$_{unique}$	26238	6027	11764	40891
R_{int}	–*	0.0484	0.00528	0.0953
parameters/restrains	2485/2769	472/123	1649/2390	1963/364
Goodness-of-fit (F^2)	1.071	1.662	1.441	1.012
R [$I > 2\sigma(I)$]	0.1012	0.0723	0.1788	0.0673
wR^2 [$I > 2\sigma(I)$]	0.2343	0.2279	0.3584	0.1374
R_{total}	0.2213	0.0989	0.2287	0.1639
wR^2_{total}	0.2630	0.2397	0.3822	0.1716
diff. peak/hole	1.280 / –0.686	1.235 / –1.127	3.269 / –1.308	0.652 / –0.716

(e Å^{-3})				

* Multidomain. Refined as a 3

The crystal structure of **CP2** is formed by zig-zag 1D chains along the *c* axis, built from the repeating unit [Cu_2(calix)$_2$] (Figure 2a). The copper atoms form the typical {Cu_2(carboxylate)$_4$} dimer (Cu–Cu distance = 2.66 Å), with the four bridging carboxylates belonging to two different **L2** molecules. These neutral chains form a pseudo-tetragonal packing, with all Cu–Cu axis along the *c* direction, and with orthogonal orientation between adjacent chains (Figure 2b). Solvent molecules, in this case DEF, occupy the axial positions on the Cu dimers. The four pyrrole rings point their NHs towards the calix cavity in a convergent manner, strongly binding a solvent molecule (DEF) by establishing four simultaneous hydrogen bonds with the oxygen atom of the latter.

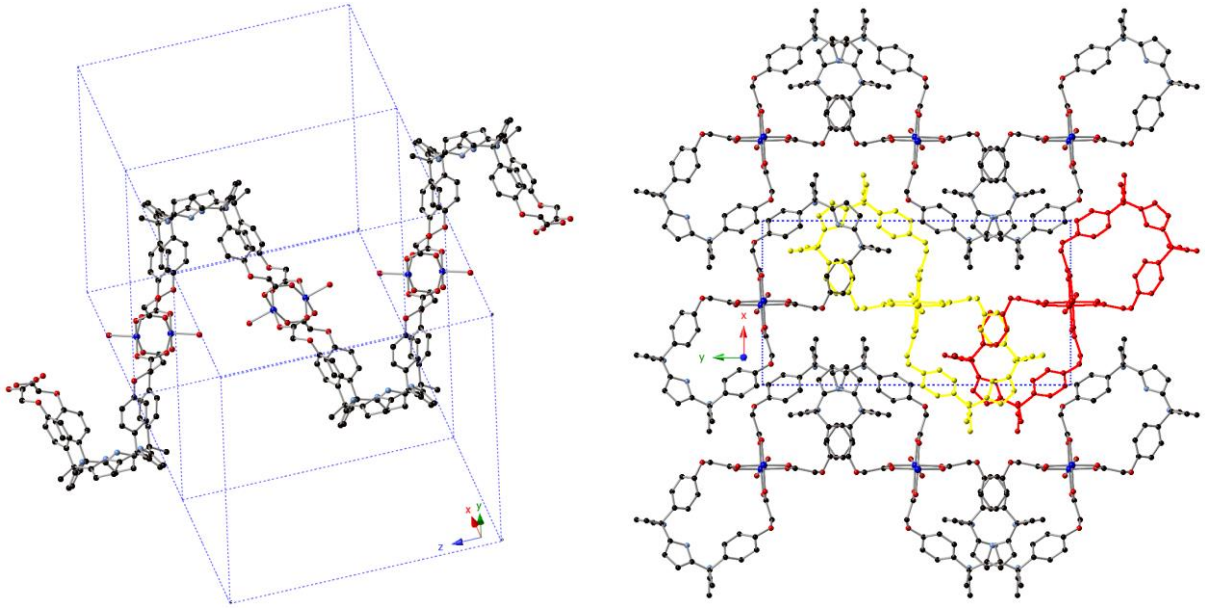

a) b)

Figure 2. Representation of the crystal structure of **CP2**: a) View of the chain structure along the *c* axis; b) Projection on the *ab* plane, highlighting the two orientations of the chains in red and yellow.

2.2.1.1 Effect of the solvent on the assembly of **L2** induced by coordination to Cu^{II}. As shown above, the coordination networks in **CP2** display the calix[4]pyrrole ligands, **L2**, in the cone conformation and with one DEF molecule deep included. Four-wall aryl-extended calix[4]pyrroles, which are structurally closely related to **L2** are known to adopt preferentially an alternate conformation in solutions of non-polar chlorinated solvents, in which only two NHs of the pyrrole rings converge. In this conformation, the receptor does not have well-defined aromatic cavities. Conversely, the same compounds in solution of polar solvents with suitable sizes and hydrogen-bond acceptor moieties i.e. DMF, acetone or CH_3CN adopt the cone conformation, in which all the NH groups converge into the deeper aromatic cavity defined by this conformation and establish four simultaneous hydrogen bonds with the oxygen atom of the included solvent molecule. Single crystals of aryl-extended calix[4]pyrroles grown from polar solvents also show the receptor in the cone conformation with one included solvent molecule.[26]

In the case of **CP2**, the solid-state structure nicely shows that the included DEF molecule in **L2** forms four simultaneous hydrogen bonds between its oxygen atom and the four NHs of the pyrrole rings of the calix core (Figure 3a). We measured an average distance of 3.02 Å for the N···O interactions supporting the formation of strong hydrogen bonds. Moreover, the inclusion complex DEF@**L2** is stabilized by multiple additional CH-π interactions i.e. d(OHC···$Ar_{centroid}$) = 3.60 Å and ($EtNCH_3H_2C$···$Ar_{centroid}$) = 3.54 Å. The calix[4]pyrrole **L2** as component of the **CP2** adopts the cone conformation and defines a closed polar cavity (Figure 3b). The cavity is closed on the bottom by the calix[4]pyrrole core and on the top by one molecule of DEF disordered in two positions, and two water molecules axially coordinated to each one of the two inwardly oriented Cu atoms of the paddle wheels stabilizing the capsular dimer. Closing the cavity of **L2**, there is also a bridging hydrogen bonded water molecule and a pyrrole ring of an adjacent **L2** unit. The

volume of the cavity was computed to be 167 $Å^3$ (purple surface in Figure 3b) using the Swiss-PdbViewer 4.1.0 software. In turn, the volume of DEF calculated with the same software is 109 $Å^3$, which allows the calculation of a packing coefficient value (PC) of 65% for the encapsulation complex of DEF@**L2** in the solid state. The calculated PC value is slightly larger than the 55% value described by Rebek *et al.* as ideal value for encapsulation complexes in solution and in non-polar cavities.[27] We have observed PC values as large as 75% for encapsulation complexes of *N*-oxides in calix[4]pyrrole-based capsules.[28] The existence of strong polar interactions between the cargo and the container allows PC values larger than the ideal 55% in the resulting encapsulation complexes.

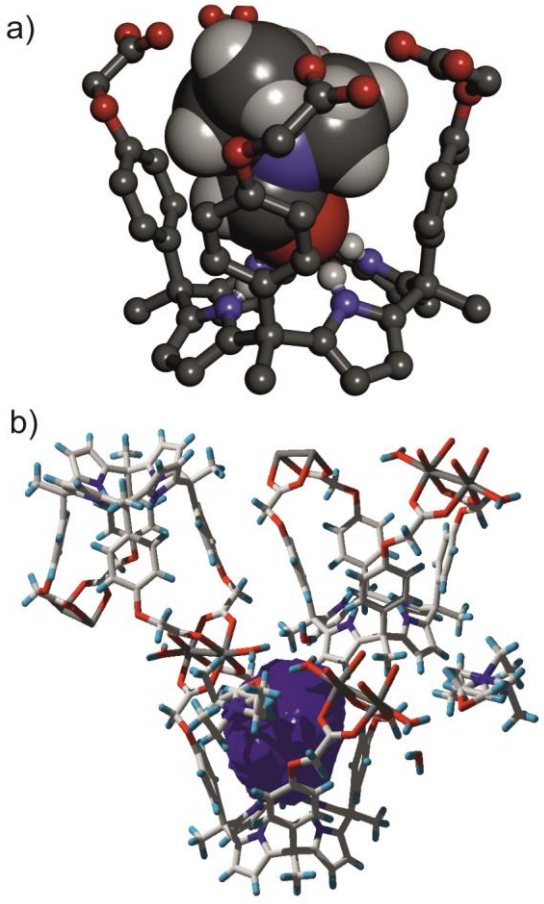

Figure 3. a) X-ray structure of the inclusion complex DEF@**L2** forming the 1D coordination polymer **CP2** through the assembly of two divergent $Cu^{II}_2(O_2CR)_4$ paddle wheels as SBUs. For

clarity, the DEF disorder and the non-polar hydrogen atoms of **L2** were removed. **L2** is shown in ball-and-stick representation and the included DEF molecule as CPK model; b) Selected section of the crystal-packing of **CP2** that was used to calculate the volume of the polar cavity of **L2** including the DEF molecule.

Interestingly, all our attempts to assemble **L2** in a metal-organic material with Cu^{II} but using DMF as solvent produced a crystalline solid with completely different morphology. The X-ray solution of the diffracted data obtained from sub-optimal single crystals displayed the presence of metal-mediated discrete dimeric cages of **L2**, **C2** (Figure 4). The cage assembly, is neutral and its covalent structure is based on two square-four connected units $Cu^{II}_2(O_2CR)_4$, *a.k.a* as Cu^{II} paddle wheels, that bridge two **L2** tetra-carboxylate ligands. The capsular container, **C2**, presents two polar hemispheres with one included DMF molecule. The two hemispheres are separated by the two inwardly directed water molecules axially coordinated to the $Cu^{II}_2(O_2CR)_4$ units. Each one of the two internal water molecules is hydrogen bonded to a DMF molecule closing the polar aromatic cavities of the two capsular hemispheres. The computed volumes for the capsular hemispheres of **C2** were 136 $Å^3$ (blue) and 134 $Å^3$ (green), respectively. (Figure 4)

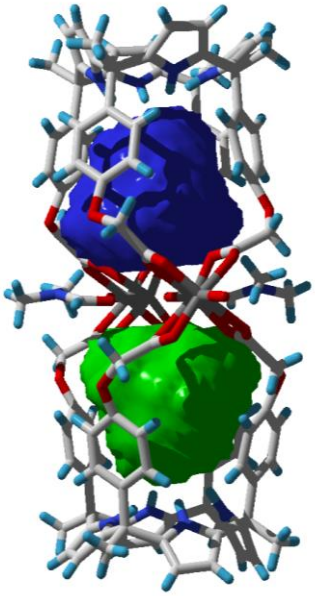

Figure 4. Solid-state structure of the dimeric capsular assembly DMF_2⊂**C2**. The included DMF molecules were removed in order to calculate the volumes of the two separate polar cavities of the capsule.

The encapsulation of one DMF molecule (74 $Å^3$) in each of the two hemispheres provides ideal PC values of 55% for the resulting encapsulation complex. The putative dimeric capsular assembly encapsulating DEF, DEF_2@**C2**, would have PC values *c.a.* to 81% suggesting that the assembly should not be thermodynamically favored based on the cargo/container volume ratio or complementarity. For the same token, the putative linear coordination polymer, DMF⊂**CP2**, which would result from the inclusion of DMF in **L2** instead of DEF, would result in a PC value of 44%. This estimated value is significantly below the ideal range of 55-70% that is expected for thermodynamically stable encapsulation complexes. In short, we surmise that the observed switching in morphology of the metal-assembly of **L2** mediated by square connected $Cu^{II}_2(O_2CR)_4$ units, from a zig-zag coordination polymer DEF⊂**CP2** to a discrete metallo-capsular assembly

DMF_2⊂**CuC2**, is mainly due to volume complementarity. The polar cavity of **L2** defined in the corresponding metallo-assembled solids adapts to the volume of the included solvent molecule by changing the ligand's coordination mode.

2.2.2 C2 and C3 dimeric metallocages.

Remarkably, **C2** shows an analogous molecular structure to **C3**, which was assembled under identical conditions using ligand **L3** (Figures 5 and 6). Both solids are composed of discrete neutral molecules assembled by dimerization of the ligands, **L2** or **L3**, through two Cu^{II}_2-$(O_2CR)_4$ paddle wheels as SBUs. In **C2,** the capsules pack in orthogonal orientations with respect to their long axis, with the calix[4]pyrrole cavities pointing to each other between adjacent units (Figure 5b,c). The capsules leave empty spaces among them that are occupied by disordered solvent molecules (DMF).

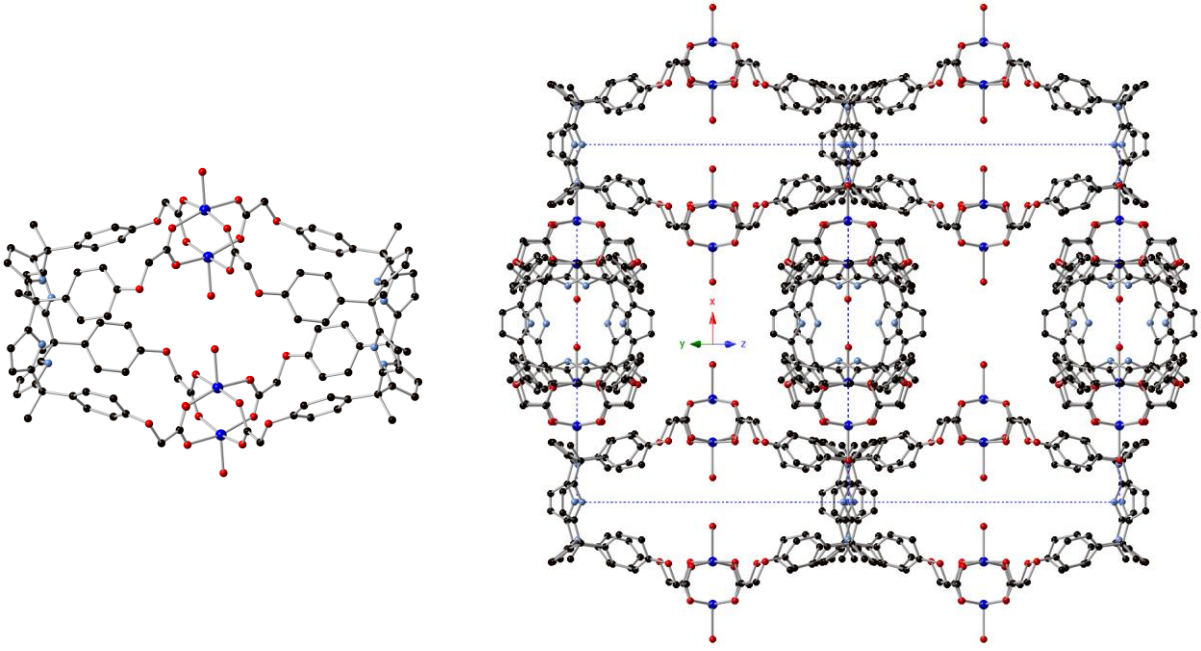

a) b)

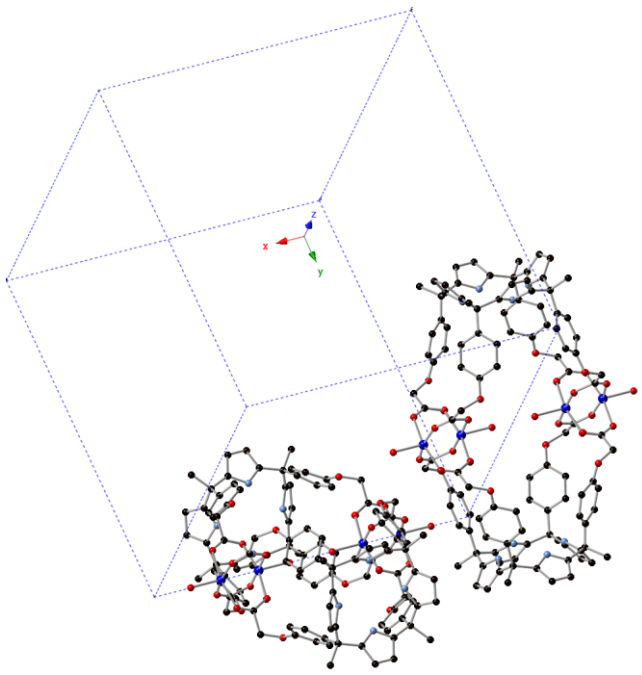

c)

Figure 5. Representation of the crystal structure of **C2:** a) Representation of the capsule; b) projection on the [011] plane; c) Detail showing the respective orientation between two adjacent capsules.

In contrast, the packing of **C3** show all capsules packed parallel to each other with respect to their long axis (Figure 6b,c). A second difference is the lack of an axial water molecule in the corresponding interior position of the Cu_2 dimers, with an inter-dimer Cu–Cu distance of just 3.281 Å. This very short contact precludes the presence of any ligand in these positions. We assign this to the conformational flexibility of the ligand arms in **L3**, which allows a closer contact between the two paddle-wheel units of the capsule and the establishment of Cu···O interactions. The shorter arms of the **L2** ligand do not allow for this close contact. On the outer axial positions of the Cu_2^{I}-paddle wheels in **C3** there is a bound solvent (DMF) molecule. The parallel orientation of all **C3** capsules is also due to their higher conformational flexibility. The phenyl rings define the shortest

contact between **C3** capsules. A C–C distance below 4.2 Å suggests the presence of aromatic interactions favoring this parallel orientation.

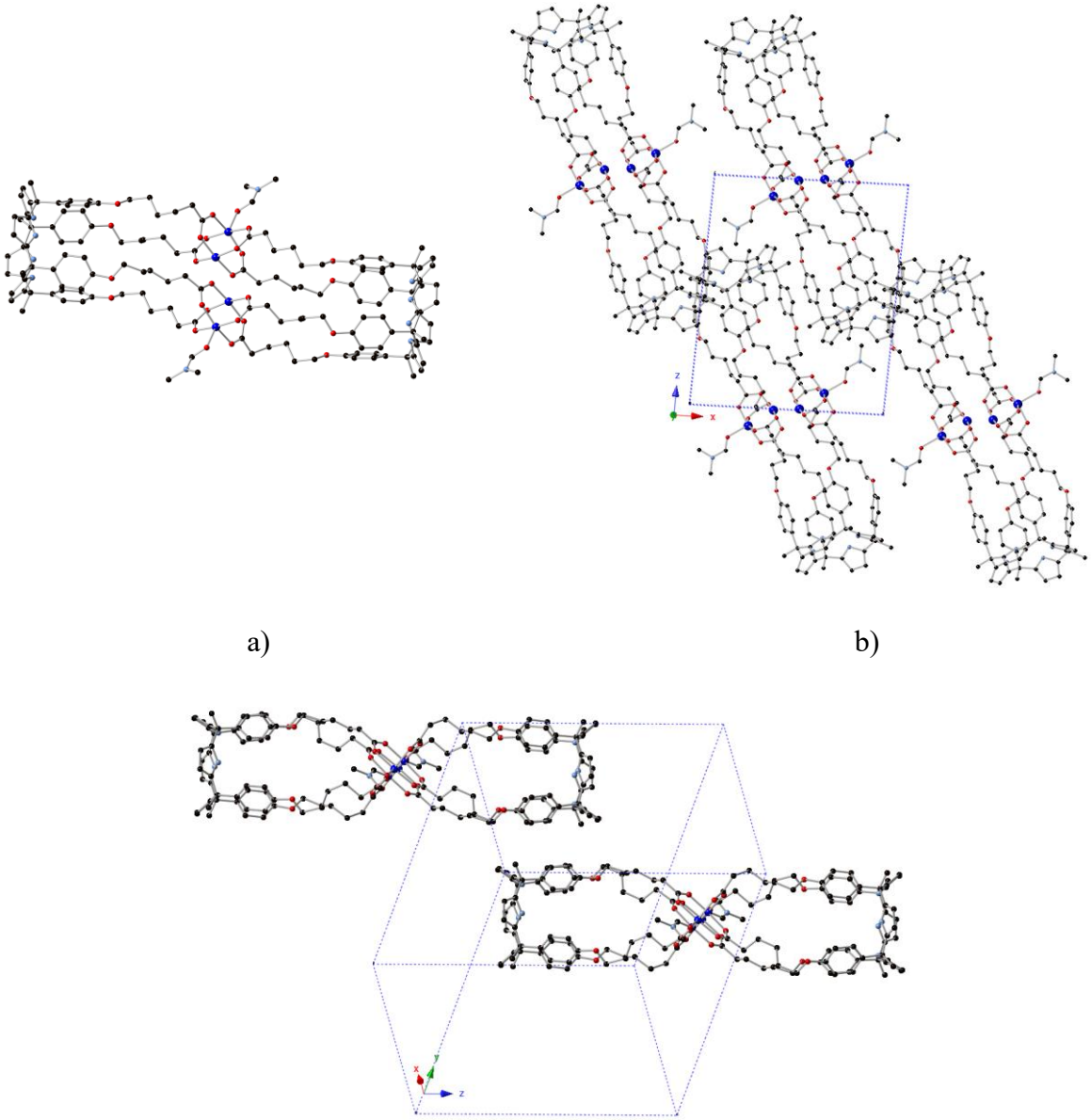

a) b)

c)

Figure 6. Representation of the crystal structure of **C3:** a) Representation of the capsule; b) Projection on the *ac* plane; c) Detail showing the respective orientation between two adjacent capsules.

2.2.2.1 Effect of the solvent on the on the assembly of **L3** induced by coordination with Cu^{II}.

The analysis of the volume complementary for the two hemispheres in the dimeric metallo-capsular assembly $(DMF)_2$@**C3** (Figure 7) produced calculated PC values of 70%, which are near the maximum of the ideal PC range determined for thermodynamically stable encapsulation complexes of polar molecules.[28] Unfortunately, using identical experimental conditions but replacing DMF by DEF as solvent in the solvothermal assembly of **L3** mediated by Cu^{II} did not produce any crystalline metal-organic solid.

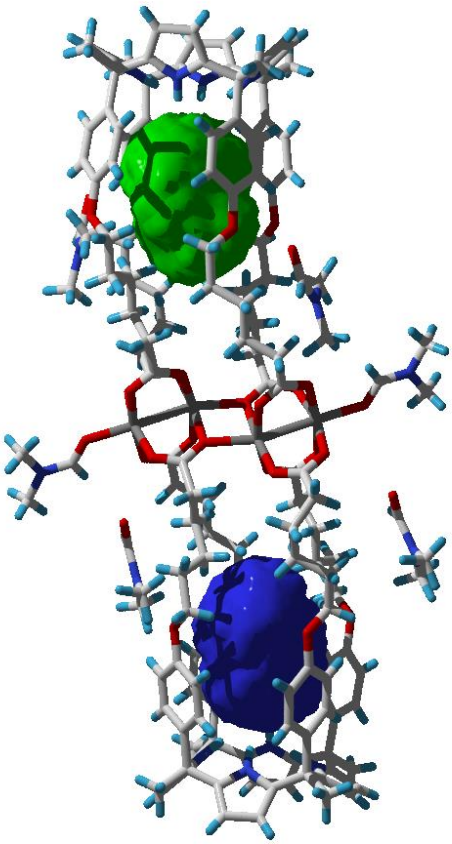

Figure 7. Solid-state structure of the capsular assembly DMF_2⊂**CuC3**. The included DMF molecules were removed before the calculation of the volumes of its two polar cavities. Four DMF

molecules were strategically located in the periphery of the capsule to avoid the escape of the sphere used to measure the cavity volumes. In the packing of the crystal, the cavities are closed by adjacent packed capsules.

2.3 Thermal analysis. We studied the thermal stability of the metal-organic compounds **MOF1** and **CP2**. Thermogravimetric analyses (TGA) were carried out in polycrystalline samples under nitrogen atmosphere (Figure S3 and S4). Both compounds showed a small solvent loss (5-10%) below 100 ºC, that we assigned to uncoordinated water molecules. No additional solvent loss was observed until decomposition of the material started, above 200 ºC. According to these results, the DMF and DEF molecules in the solid structure, particularly those included and hydrogen-bonded to the NHs of the calix[4]pyrrole cores, were not removed under these conditions. Thus, although the volume occupied by solvent molecules in the crystal structure is significant (close to 39% of the crystal volume, 2640 $Å^3$ per unit cell, for **MOF1** and 24% of the crystal volume, 1470 $Å^3$ per unit cell, for **CP2**),[29] the complex removal of the solvent molecules makes difficult to exploit their intrinsic porosity. BET (Brunauer-Emmett Teller) analyses through nitrogen adsorption isotherms indicate negligible porosity (Figures S5 and S6 in the SI). We attempted the removal of the solvent molecules through other methods, including combination of heat and high vacuum, or substitution with more volatile solvents. However, all our attempts failed to improve DMF/DEF removal.

2.4 Magnetic Characterization. Since the paramagnetic Cu^{2+} centers (S = 1/2) are connected through carboxylate bridging ligands in the $Cu^{II}_2(O_2CR)_4$ SBUs, we decided to study their magnetic properties to determine the superexchange interactions present in these compounds. Magnetically, **CP2**, **C2** and **C3** are identical, both contained the classic and well-studied $Cu^{II}_2(O_2CR)_4$ paddle wheel.[30] In these complexes, a strong antiferromagnetic superexchange stabilizes the singlet ground state.[31] This is at the origin of a broad maximum observed in the

magnetic susceptibility *vs* temperature plot above 150 K (Figure 8). Since the two compounds showed negligible differences in their magnetic behavior, we present here only the modeled magnetic data for **C2**. The magnetic interaction between the two Cu centers (S_1 = 1/2, S_2 = 1/2) can be simulated with a simple Hamiltonian;

$$H = -2J(S_1S_2) \quad (1)$$

that takes into account isotropic magnetic coupling between magnetic centers. A satisfactory fit of the experimental data is achieved with the inclusion of a small paramagnetic contribution ($\chi_{para} = C/T$) that accounts for the appearance of the Curie tail at very low temperatures (Figure 8). This is typical of antiferromagnetically coupled compounds, and responds to the presence of crystal defects or small impurities. The magnetic parameters obtained, g = 2.16 and J = –115 cm^{-1} (C = 0.04 emu mol^{-1}, ≈ 5% paramagnetic impurity), are in very good agreement with previous data.[26]

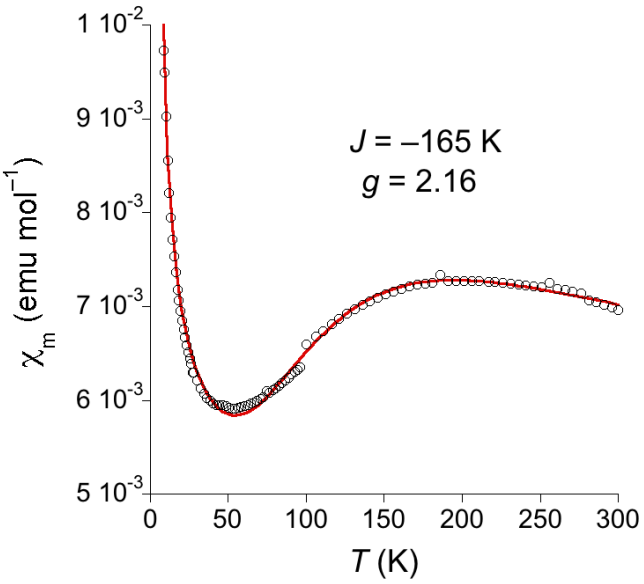

Figure 8. Magnetic susceptibility (χ_m) for **C2** as a function of temperature (circles), and the fitting to a singlet-triplet model.

The magnetic behavior of **MOF1** is quite different. It contains a rhomb-like tetracopper unit, with two different bridges. The Cu–Cu distances are 2.868 Å along the short diagonal, and 3.296 Å

along the sides. These are significantly longer than in the Cu_2 paddle wheel (2.63 Å). In addition, the CuO_4 conformation is highly distorted from square planar, with one oxygen atom at over 1 Å from the plane defined by the other three (in contrast, the four O atoms defining a perfect plane in **C2**). The molecular bridges are also different, with a double μ_2-hydroxy square Cu_2O_2 (Cu–O–Cu = 96º) in the short diagonal. The side bridges are formed by a double hydroxy/carboxylate connecting Cu centers in two different geometries (square planar vs distorted trigonal bipyramid). All these structural features suggested that weaker magnetic coupling was expected for this case, due to the mismatch between magnetic orbitals. Additionally, the triangular arrangement around the μ_3-hydroxy bridges may give rise to spin frustration.

The $\chi_m T$ product at room temperature, 1.65 emu K mol^{-1}, matches the expected spin-only value (1.50 emu K mol^{-1}). When lowering the temperature $\chi_m T$ decreases slowly below 150 K, and faster below 60 K, suggesting the presence of antiferromagnetic coupling between paramagnetic centers. As a reasonable first approximation, the magnetic superexchange along the long diagonal can be neglected. Using this approximation, the magnetic data can be modeled with the following Hamiltonian:

$$H = -2J(S_1S_2 + S_1S_3 + S_2S_4 + S_3S_4) - 2J'(S_2S_3) \quad (2)$$

where $S_1 = S_2 = S_3 = S_4 = 1/2$. The best fitting was found for $g = 2.05$, $J = -5.6$ cm^{-1}, and $J' = -13.9$ cm^{-1}, with the short diagonal superexchange parameter being 2-3 times stronger than the rhomb-side one. With these parameters, the high temperature data is perfectly reproduced, but the model deviates at very low temperatures, where the experimental $\chi_m T$ product is higher. We assign this to the presence of paramagnetic impurities (see above), although we did not attempt to add this contribution to the model to avoid overparametrization. The results are in good agreement with the expected behavior from the molecular structure: all superexchange interactions are

antiferromagnetic although much weaker in this case. Indeed, no maximum is observed in the χ_m vs T plot (Figure 9).

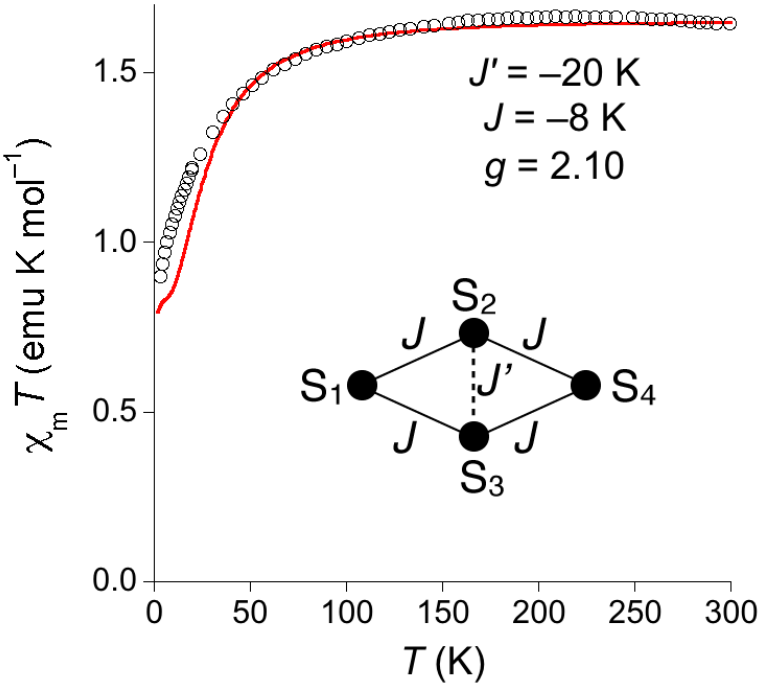

Figure 9. Temperature dependence of the $\chi_m T$ product for **MOF1** (circles), and the fitting to a rhomb-like model (eq. 2).

3. CONCLUDING REMARKS

In summary, we reported the preparation of four calix[4]pyrrole-based metal-organic compounds. We show that in some of the reported structures, the coordination mode of the organic likers and the structure of the Cu^{II}-carboxylate clusters acting as secondary building unit (SBU) are dominated by two factors. These are the anchoring position of the carboxylic group attached to the aryl moiety of the calix[4]pyrrole (i.e. *meta*- or *para*-position) and the solvent used in their solvothermal synthesis. The former was expected, but the latter is much subtler and delicate. The solvent effect is illustrated by the possibility of switching from discrete calix[4]pyrrole capsules

found in **C2** to a 1D zig-zag coordination polymer constituting **CP2**, by just changing the solvent used in their syntheses from DMF to DEF, respectively. This minor modification promotes a completely different structure of the solid. We assign this surprising result to the solvent (DMF or DEF) recognition by the host molecules used as organic linkers, which in turn pre-organizes the calix[4]pyrrole core of the ligand in the cone conformation but with a substantial different filling of its polar cavity volume. This modulates the preferred orientation of the aryl-substituted carboxylic groups in **L2**, prior to self-assembly, during crystal growth and dictates the preferential formation of dimers (**C2**) or the polymer (**CP2**) observed in the crystals. The obtained results highlight the strong interplay that exists between molecular recognition, supramolecular isomerization and solid-state structure. Conformational control of the linker substituents through binding to solvent molecules or other guests prior to self-assembly can give rise to the expected and/or unexpected solid-state architectures that may be further developed for sensing and/or catalysis applications.

4. EXPERIMENTAL SECTION

Characterization. ^{1}H-NMR and ^{13}C-NMR spectra were recorded on a Bruker Avance 400 (400 MHz for ^{1}H-NMR) or on a Bruker Avance 500 (500 MHz for ^{1}H-NMR). Deuterated solvents were purchased from Aldrich. Chemical shifts are given in ppm. Hight resolution mass spectra were obtained on a Micro TOF II (Bruker Daltonics) ESI as ionization mode mass spectrometer. Powder X-Ray (PXRD) data were collected with a D8 Advance Series 2θ/θ powder diffractometer at room temperature BET: N_2 adsorption/desorption isotherms were measured at 77 K using an AutosorbiQ after the sample was first degassed under vacuum at 120 ºC overnight. Surface areas were determined by the BET method in an appropriate pressure range. Thermogravimetric analyses

were performed with a TGA/SDTA851 Mettler Toledo instrument at a heating rate of 5 °C min^{-1} between 30 and 800 °C under a constant flow of air (50 mL min^{-1}). Magnetic susceptibility measurements between 2 and 300 K were carried out in a Quantum Design MPMS-XL SQUID magnetometer using a 1000 Oe field. Pascal's constants were used to estimate the diamagnetic corrections for the compounds.

Crystal structure determination. X-Ray diffraction data were collected on a Rigaku XtaLab P200 Mo *Kα* rotating anode equipped with a Pilatus 200K hybrid pixel detector equipped with an Oxford Cryostream 700 plus low temperature device. Data collection were carried out using CrystalClear-SM Expert 2.1 b29.[32] For the data reduction and absorption correction CrysAlisPro 1.171.38.37f was used.[33] Structure solution was obtained with the VLD algorithm under SIR2011.[34] Structure refinement was performed with SHELXL-2014.[35] For the structure MOF1 the program PLATON SQUEEZE[36] was used for treating highly disordered solvent accessible voids. CCDC 1519366 (**C2**), 1519369 (**C3**), 1519368 (**MOF1**) and 1519367 (**CP2**) contain the supplementary crystallographic data for this paper.

Synthesis. All solvent and reagents used in the synthesis of the described compounds were purchased from commercial sources and were used without further purification.

Calix[4]pyrrole 1 (see SI for the structure): This compound was prepared accordingly to the procedure described by Ballester *et al*.[37] with slightly modifications**:** Briefly In a round bottom flask, 4'-hydroxyacetophenone (10 g, 73.4 mmol), pyrrole (5.35 mL, 77 mmol) and ethyl acetate (735 mL) were added. HCl 36% (62.5 mL, 734 mmol) was slowly added. The mixture was stirred under air overnight. To quench the reaction, 150 mL of water were added. Solid KOH was added until pH 6 and then further neutralized with solid K_2CO_3 until pH 7. The organic phase was separated, washed twice with water, dried over Na_2SO_4, filtered and concentrated under reduced

pressure. The residue was dissolved in Et_2O (300 mL) and after filtration of insoluble impurities, the filtrate was concentrate under reduced pressure. The crude was dissolved in dichloromethane (250 mL), and the solution was left overnight at room temperature to obtain a white precipitate of **1** that was collected and recrystallized from acetonitrile to yield colorless crystals. Yield = 30 %. ^{1}H-NMR spectrum is in agreement with the previously described by Ballester *et al*.

Calix[4]pyrrole 2 (see SI for the structure): Compound **1** (3 g, 4.05 mmol) and K_2CO_3 (4.48 g, 32.4 mmol) were suspended in dry 150 mL DMF. Under stirring, methyl-2-bromoacetate (2.98 mL, 32.4 mmol) was dropwise added. The suspension was heated at 70 ºC overnight. Next, the solution was cooled down, filtered and the solvent evaporated. Distilled water was added to the solution and the organic product was extracted with dichloromethane, dried over Na_2SO_4, filtered and the solvent removed *in vacuo*. Finally, the brownish precipitated was triturated with MeOH:hexane (95:5) which gave the compound **2** in 71% yield. ^{1}H-NMR (400 MHz, *d*-acetone): δ 8.92 (br s, 4H , pyrrole-N*H*), 7.22 (app t, *J* = 7.58 Hz, 4H, Ar*H*), 6.67-6.53 (m, 12H, Ar*H*), 6.01 (d, *J* = 2.56 Hz, 8H, β-pyrrole), 4.67 (s, 8H, CH_2), 3.76 (s, 12H, CH_3), 1.89 (s, 12H, CH_3). ^{13}C-NMR (400 MHz, d-acetone) δ 169.9, 158.8, 152.6, 138.1, 130.1, 121.4, 115.6, 111.7, 106.1, 65.6, 52.2, 45.4, 30.9 HRMS (ESI) m/z 1051.4106 $(M + Na)^+$ calcd for $C_{60}H_{60}N_4NaO_{12}$, found 1051.4118.

Calix[4]pyrrole L1: Calix[4]pyrrole **2**, (3 mmol) was dispersed in 80 mL THF:H_2O (1:1) and stirred vigorously while lithium hydroxide (18 mmol) was added. After 1 h of stirring, the tetrahydrofurane was evaporated under reduced pressure and the aqueous solution was acidified with HCl 1N. A precipitate appears which was extracted with ethyl acetate (120 mL). The organic layers were dried over Na_2SO_4 and evaporated under reduced pressure to yield the pure product. Yield = 81 %. ^{1}H-NMR (400 MHz, *d*-acetone): δ 8.91 (br s, 4H , pyrrole-N*H*), 7.25 (app t, *J* =

8.29 Hz, 4H, Ar*H*), 6.69-6.55 (m, 12H, Ar*H*), 6.01 (d, *J* = 2.55 Hz, 8H, β-pyrrole), 4.65 (s, 8H, CH_2), 3.76 (s, 12H, CH_3).

Calix[4]pyrrole 3 (see SI for the structure): This compound was prepared accordingly to the procedure described by Sessler *et al*.[38] with slightly modifications**:** Briefly, in a round bottom flask equipped with a magnetic bar and under N_2 atmosphere, 4'-hydroxyacetophenone (10 g, 72.7 mmol) and pyrrole (5.08 mL, 72.7 mmol) were dissolved in methanol (150 mL). Methanesulfonic acid (1.3 mL, 20 mmol) was slowly added via syringe under stirring. The reaction was stirred at room temperature overnight. To quench the reaction, 200 mL of water were added forming a black tar that was recovered by filtration, dissolved in 100 mL of diethyl ether (helped by ultrasounds). After filtering through a pleated filter paper, the mixture was concentrated under vacuum to yield a red foam-like material. The desired isomer is recrystallized from glacial acetic acid as colorless crystals in 45 % yield (13.4 g). ^{1}H-NMR spectrum is in agreement with the previously described by Sessler *et al*.

Calix[4]pyrrole 4 (see SI for the structure): Compound **3** (3 g, 4.05 mmol) and K_2CO_3 (4.48 g, 32.4 mmol) were suspended in dry 150 mL DMF. Under stirring, methyl-2-bromoacetate (2.98 mL, 32.4 mmol) was dropwise added. The suspension was heated at 70 ºC overnight. Next, the solution was cooled down, filtered and the solvent evaporated. Water was added to the crude and the organic product was extracted with dichloromethane, dried over Na_2SO_4, filtered and the solvent removed *in vacuo*. Finally, the brownish precipitated was triturated with MeOH which gave the compound **4** in 86 % yield. ^{1}H-NMR (400 MHz, *d*-acetone): δ 8.85 (br s, 4H , pyrrole-N*H*), 6.92-6.80 (m, 16H, Ar*H*), 6.00 (d, *J* = 2.58 Hz, 8H, β-pyrrole), 4.70 (s, 8H, CH_2), 3.78 (s, 12H, CH_3), 1.83 (s, 12H, CH_3). ^{13}C-NMR (400 MHz, d-acetone)

169.2, 156.7, 143.0, 137.5, 128.3, 114.0, 104.8, 64.7, 51.5, 43.9, 30.3. HRMS (ESI) m/z 1051.4106 $(M + Na)^+$ calcd for $C_{60}H_{60}N_4NaO_{12}$, found 1051.4107.

Calix[4]pyrrole 5 (see SI for the structure): Compound **3** (0.3 g, 0.405 mmol) and K_2CO_3 (448 mg, 3.24 mmol) were suspended in dry 15 mL DMF. Under stirring, ethyl-6-bromohexanoate (0.576 mL, 3.24 mmol) was added. The suspension was heated at 70 ºC overnight. Next, the solution was cooled down, filtered and the solvent evaporated. Water was added to the solution and the organic product was extracted with dichloromethane, dried over Na_2SO_4, filtered and the solvent removed *in vacuo*. Finally, the brownish precipitated was recrystallized from EtOH which gave the compound **5** in 60 % yield. ^{1}H-NMR (400 MHz, *d*-acetone): δ 8.81 (br s, 4H , pyrrole-N*H*), 6.91-6.81 (m, 16H, Ar*H*), 6.00 (d, *J* = 2.40 Hz, 8H, β-pyrrole), 4.11 (q, *J* = 7.08 Hz, 8H, C*H*$_2$CH$_3$), 3.95 (t, *J* = 6.00 Hz, 8H, CH$_2$C*H*$_2$), 2.35 (t, *J* = 7.27 Hz, 8H, C*H*$_2$CH$_2$), 1.86 (s, 12H, C*H*$_3$), 1.82-1.74 (m, 8H, C*H*$_2$CH$_2$CH$_2$), 1.73-1.64 (m, 8H, C*H*$_2$CH$_2$CH$_2$), 1.55-1.48 (m, 8H, C*H*$_2$CH$_2$CH$_2$), 1.25 (t, J = 7.43 Hz, 12H, CH$_2$C*H*$_3$), ^{13}C-NMR (400 MHz, d-acetone) δ 172.8, 157.6, 142.6, 138.1, 128.9, 113.7, 104.5, 67.7, 61.9, 59.4, 43.9, 33.7, 32.6, 25.2, 24.6, 13 .8. HRMS (ESI) m/z 1331.7235 $(M + Na)^+$ calcd for $C_{80}H_{100}N_4NaO_{12}$, found 1331.7519

Calix[4]pyrrole L2: Calix[4]pyrrole **4,** (3.35 mmol) was dispersed in 100 mL THF:H_2O (1:1) and stirred vigorously while lithium hydroxide (20.11 mmol) was added. After 1 h of stirring, the tetrahydrofurane was evaporated under reduced pressure and the aqueous solution was acidified with HCl 1N. A precipitate appears which was extracted with ethyl acetate (150 mL). The organic layers were dried over Na_2SO_4 and evaporated under reduced pressure to yield the pure product. Yield **L2** = 90 %, ^{1}H-NMR (400 MHz, *d*-acetone): δ 8.84 (br s, 4H , pyrrole-N*H*), 6.92-6.81 (m, 16H, Ar*H*), 6.00 (d, *J* = 2.66 Hz, 8H, β-pyrrole), 4.68 (s, 8H, C*H*$_2$), 1.83 (s, 12H, C*H*$_3$).

Calix[4]pyrrole L3 was obtained by using the same procedure than **L2** but starting from calix[4]pyrrole **5**. Yield **L3** = 91 % ^{1}H-NMR (400 MHz, *d*-acetone): δ 8.77 (br s, 4H , pyrrole-N*H*), 6.91-6.80 (m, 16H, Ar*H*), 5.97 (d, *J* = 2.57 Hz, 8H, β-pyrrole), 3.94 (t, *J* = 6.35 Hz, 8H, CH_2CH_2), 2.35 (t, *J* = 7.21 Hz, 8H, CH_2CH_2), 1.85 (s, 12H, CH_3), 1.82-1.74 (m, 8H, $CH_2CH_2CH_2$), 1.73-1.62 (m, 8H, $CH_2CH_2CH_2$), 1.57-1.48 (m, 8H, $CH_2CH_2CH_2$).

MOF-1: 400 mg of **L1** (0.411 mmol) and 45 mg of $Cu(NO_3)_2$ x H_2O (0.205 mmol, ratio ligand:metal 2:1) were dissolved in 45 mL of DMF and carefully layered on 21 mL of deionized H_2O. The mixture is heated in a Teflon-lined autoclave at 100 ºC for 24 h. The resulting blue precipitate was filtered, washed with DMF and EtOH, and finally dried at 80 ºC for 24 h. Yield = 63 mg

CP-2: 300 mg of **L2** (0.307 mmol) and 37 mg of $Cu(NO_3)_2$ x H_2O (0.154 mmol) were dissolved in 35 mL of DMF and carefully layered on 17.5 mL of deionized H_2O. The mixture is heated in a Teflon-lined autoclave at 100 ºC for 24 h. The resulting blue precipitate was filtered, washed with DMF and EtOH, and finally dried at 80 ºC for 24 h. Yield = 58 mg

Capsule C2: 800 mg of **L1** (0.822 mmol) and 99 mg of $Cu(NO_3)_2$ x H_2O (0.411 mmol, ratio ligand:metal 2:1) were dissolved in 90 mL of DMF and carefully layered on 45 mL of deionized H_2O. The mixture is heated in a Teflon-lined autoclave at 100 ºC for 24 h. The resulting blue precipitate was filtered, washed with DMF and EtOH, and finally dried at 80 ºC for 24 h. Yield = 155 mg

Capsule C3: 23.5 mg of **L3** (0.021 mmol) and 2.5 mg of $Cu(NO_3)_2$ x H_2O (0.001 mmol, ratio ligand:metal 2:1) were dissolved in 2 mL of DMF and carefully layered on 1 mL of deionized H_2O. The mixture is heated in a Teflon-lined autoclave at 100 ºC for 24 h. The resulting blue

precipitate was filtered, washed with DMF and EtOH, and finally dried at 80 ºC for 24 h. Yield = 9 mg

ASSOCIATED CONTENT

Supporting Information. The following files are available free of charge. PXRD, TGA, BET, ^{1}H-NMRs, details on the disorder models for structures **C2** and **MOF1** and additional magnetic data.

AUTHOR INFORMATION

Corresponding Author

jrgalan@iciq.es; pballester@iciq.es.

Author Contributions

The manuscript was written through contributions of all authors. All authors have given approval to the final version of the manuscript.

ACKNOWLEDGMENT

We are thankful for the financial support of the EU (ERC Stg Grant 279313, CHEMCOMP); the Spanish Ministerio de Economía y Competitividad (MINECO) through projects CTQ2015-71287-R, CTQ2014-56295-R and the Severo Ochoa Excellence Accreditation 2014-2018 SEV-2013-0319, FEDER funds (project CTQ2014-56295-R), and the Generalitat de Catalunya (2014-SGR-797, and CERCA Programme).. JAS gratefully thanks the Marie Curie COFUND Action from the European Commission for cofinancing his postdoctoral fellowship. We also thank one of the reviewers for noticing us the topological type of MOF1. The corresponding information is included in reference 25.

REFERENCES

[1] Kitagawa, S.; Kitaura, R.; Noro, S.-i., *Angew. Chem. Int. Ed.* **2004,** *43*, 2334-2375.

[2] Cheetham, A. K.; Rao, C. N. R.; Feller, R. K., *Chem. Commun.* **2006**, 4780-4795.

[3] Li, J.-R.; Kuppler, R. J.; Zhou, H.-C., *Chem. Soc. Rev.* **2009,** *38*, 1477-1504.

[4] Kreno, L. E.; Leong, K.; Farha, O. K.; Allendorf, M.; Van Duyne, R. P.; Hupp, J. T., *Chem. Rev.* **2012,** *112*, 1105-1125.

[5] Lee, J.; Farha, O. K.; Roberts, J.; Scheidt, K. A.; Nguyen, S. T.; Hupp, J. T., *Chem. Soc. Rev.* **2009,** *38*, 1450-1459.

[6] Schneemann, A.; Bon, V.; Schwedler, I.; Senkovska, I.; Kaskel, S.; Fischer, R. A., *Chem. Soc. Rev.* **2014,** *43*, 6062-6096.

[7] Li, X.; Chen, X.; Jiang, F.; Chen, L.; Lu, S.; Chen, Q.; Wu, M.; Yuan, D.; Hong, M., *Chem. Commun.* **2016,** *52*, 2277-2280.

[8] Walton, I. M.; Cox, J. M.; Coppin, J. A.; Linderman, C. M.; Patel, D. G.; Benedict, J. B., *Chem. Commun.* **2013,** *49*, 8012-8014.

[9] Martin, A. D.; Easun, T. L.; Argent, S. P.; Lewis, W; Blake, A.J.; Schroder, M.; *CrystEngComm* **2017**. DOI: 10.1039/C6CE01965J

[10] Huang, X.-C.; Lin, Y.-Y.; Zhang, J.-P.; Chen, X.-M., *Angew. Chem. Int. Ed.* **2006,** *118*, 1587-1589.

[11] Tian, Y.-Q.; Xu, H.-J.; Weng, L.-H.; Chen, Z.-X.; Zhao, D.-Y.; You, X.-Z., *Eur. J. Inorg. Chem.* **2004,** *2004*, 1813-1816.

[12] Coletta, M.; McLellan, R.; Murphy, P.; Leube, B. T.; Sanz, S.; Clowes, R.; Gagnon, K. J.; Teat, S. J.; Cooper, A. I.; Paterson, M. J.; Brechin, E. K.; Dalgarno, S. J., *Chem.--Eur. J.* **2016,** *22*, 8791-8795.

[13] Karagiaridi, O.; Bury, W.; Mondloch, J. E.; Hupp, J. T.; Farha, O. K., *Angew. Chem. Int. Ed.* **2014,** *53*, 4530-4540.

[14] Kim, M.; Cahill, J. F.; Su, Y.; Prather, K. A.; Cohen, S. M., *Chem. Sci.* **2012,** *3*, 126-130.

[15] Huang, X.-C.; Zhang, J.-P.; Lin, Y.-Y.; Chen, X.-M., *Chem. Commun.* **2005**, 2232-2234.

[16] Hennigar, T. L.; MacQuarrie, D. C.; Losier, P.; Rogers, R. D.; Zaworotko, M. J., *Angew. Chem. Int. Ed.* **1997,** *36*, 972-973.

[17] Kim, D. S.; Sessler, J. L., *Chem. Soc. Rev.* **2015,** *44*, 532-546.

[18] Saha, I.; Lee, J. T.; Lee, C.-H., *Eur. J. Org. Chem.* **2015,** *2015*, 3859-3885.

[19] Quinlan, E.; Matthews, S. E.; Gunnlaugsson, T., *J. Org. Chem.* **2007,** *72*, 7497-7503.

[20] Liao, W.; Liu, C.; Wang, X.; Zhu, G.; Zhao, X.; Zhang, H., *CrystEngComm* **2009,** *11*, 2282-2284.

[21] Cholewa, P. P.; Beavers, C. M.; Teat, S. J.; Dalgarno, S. J., *Cryst. Growth Des.* **2013,** *13*, 5165-5168.

[22] Bew, S. P.; Burrows, A. D.; Duren, T.; Mahon, M. F.; Moghadam, P. Z.; Sebestyen, V. M.; Thurston, S., *Chem. Commun.* **2012,** *48*, 4824-4826.

[23] Lee, E.; Kim, Y.; Heo, J.; Park, K.-M., *Cryst. Growth Des.* **2015,** *15*, 3556-3560.

[24] Lee, J.; Waggoner, N. W.; Polanco, L.; You, G. R.; Lynch, V.; Kim, S. K.; Humphrey, S. M.; Sessler, J. L., *Chem. Commun.* **2016,** *52*, 8514-8517.

[25] The topological type of MOF1 is a 4,8L15 net (the 15th 4,8-c layer net by TOPOS) with $\{4^{20}.8\}\{4_6\}_2$ point symbol. See http://topospro.com/.

[26] Gil-Ramírez, G.; Escudero-Adán, E. C.; Benet-Buchholz, J.; Ballester, P., *Angew. Chem. Int. Ed.* **2008,** *47*, 4114-4118.

[27] Mecozzi, S.; Rebek, J. J.; *Chem.--Eur. J.* **1998**, *4*, 1016-1022.

[28] Galan, A.; Espelt, M.; Ballester, P.; *Supramol. Chem.* **2016**, *28*, 455-463.

[29] A sphere of 1.2 Å of radius was calculated to be trapped in the porous.

[30] De Loth, P.; Cassoux, P.; Daudey, J. P.; Malrieu, J. P., *J. Am. Chem. Soc.* **1981,** *103*, 4007-4016.

[31] Hay, P. J.; Thibeault, J. C.; Hoffmann, R., *J. Am. Chem. Soc.* **1975,** *97*, 4884-4899.

[32] Rigaku, **2013**, CrystalClear-SM Expert 2.1 b29.

[33] Rigaku Oxford Diffraction, **2015**, CrysAlisPro Software system, version 1.171.38.37f, Rigaku Corporation, Oxford, UK.

[34] Burla, M. C.; Caliandro, R.; Camalli, M.; Carrozzini, B.; Cascarano, G. L.; Giacovazzo, C.; Mallamo, M.; Mazzone, A.; Polidori, G.; Spagna, R. *J. Appl. Cryst.* **2012**, *45*, 357-361.

[35] Sheldrick, G. M. *Acta Crystallogr., Sect. C: Struct. Chem*. **2015**, *71*, 3-8.

[36] Spek, A. L. *Acta Crystallogr., Sect. C: Struct. Chem***. 2015**, *71*, 9-18.

[37] Guinovart, T.; Hernández-Alonso, D.; Adriaenssens, L.; Blondeau, P.; Martínez-Belmonte, M.; Rius, F. X.; Andrade, F. J.; Ballester, P., *Angew. Chem. Int. Ed.* **2016,** *55*, 2435-2440.

[38] Anzenbacher, P.; Jursíková, K.; Lynch, V. M.; Gale, P. A.; Sessler, J. L., *J. Am. Chem. Soc.* **1999,** *121*, 11020-11021.

ToC: Tetraaryl-extended calix[4]pyrrole derivatives with carboxylic functional groups yield capsules, 1D chains or 2D layered structures as determined by the reaction conditions with Cu^{2+} salts.